Study of the Conducted Electromagnetic Interference in the Converter Station of an UHVDC Transmission System

Jian Le[1, *], Cao Wang[1], Hanwu Luo[2], Tao Mao[1], and Yinge Wang[1]

Abstract—The Conducted Electromagnetic Interference (CEI) characteristics in the primary circuit and at the ports of the secondary devices of the converter station of a UHVDC transmission system are researched comprehensively and systematically in this paper, by taking the Zhalute-Qingzhou $\pm 800\,\text{kV}/10000\,\text{MW}$ UHVDC project in East Inner Mongolia of China as an example. The primary circuit equipment parameters of the target system are designed systematically at first, and the overall broadband equivalent model of the main circuit of the UHVDC system, which is composed of converter valve, converter transformer, filter banks and smoothing reactor, is developed. The CEI characteristics in the primary circuit under various conditions of the UHVDC system are analyzed based on the simulations carried out on the built BEC, and the influences of several primary circuit elements on the propagation of the CEI characteristics are researched. To improve the accuracy of the analysis of the CEI characteristics in the secondary device circuit, accurate BECs of the Capacitor Voltage Transformer (CVT), Current Transformer (CT) and secondary signal cable are established. The CEI characteristics at the ports of secondary devices under different operation modes are studied, and the influences of the cable length and burden rate on the CEI characteristics are analyzed. This paper provides a comprehensive and thorough understanding of the CEI characteristics of an UHVDC system.

1. INTRODUCTION

UHVDC system fulfills an ever increasing important role in long distance and large capacity power transmission due to its large capacity, small power loss and low occupation of land [1–3]. Since 2006, four UHVDC projects have been constructed and put into operation in China, and in 2015, Eastern Inner Mongolia power company of China State Grid started the construction of 'two ACs and three DCs' UHV systems, among which the Zhalute-Qingzhou (Z-Q for short hereafter) UHVDC project starts from Zhalute in Eastern Inner Mongolia, via Inner Mongolia, Hebei, Tianjin and Shandong province, and ends at Qiongzhou in Shandong. This project is characterized by a $\pm 800\,\text{kV}$ voltage level, 10000 MW bipolar transmission capacity, about 1200 km transmission length, 2 newly built converter stations in Zhalute and Qingzhou, respectively, and plans to put into operation in 2018.

HVDC converter station has a very complex electromagnetic environment [4, 5], and the situation is even worse in an UHVDC system due to the increased electrical stress on the converter valve under a higher DC voltage level [6]. The voltage and current CEI, sourcing from the converter valve, will propagate along the primary circuit equipment and disturb the normal operations of the secondary circuit devices through coupling equipments such as CVT and CT [7]. The secondary circuit systems, consisting of the protection, control, monitoring, communication devices, etc., play a vital role in the safe operation of the UHVDC system and even the whole power system. Therefore, analyzing the CEI characteristics in the secondary circuit of the UHVDC converter station, finding the

weaknesses in secondary equipments according to the existing relevant standard [8], formulating specific electromagnetic interference protection measures, are of important theoretical and practical value to ensure the safe and stable operation of the UHVDC system in terms of electromagnetic compatibility.

Current researches regarding the CEI characteristics in an HV/UHV system mostly focus on the building of the Broadband Equivalent Circuits (BECs) of the primary circuit elements and the evaluation of CEI levels in the primary circuit. The BECs of several key primary equipments have been built in [9], and the stable operation features, CEI characteristics and its propagation have been analyzed based on time-domain simulation method. A broadband equivalent simulation model of a UHVDC converter station has been presented based on the recorded field data and the bloom circuit integration method in [10].

CEI is usually coupled from the primary circuit to the secondary side via voltage or current measuring devices such as CVT or CT. Reference [11] has analyzed the characteristics of the electromagnetic interference in the secondary circuit, which is coupled from high voltage bus through CT/CVT, or the parasitic capacitor between the primary and secondary circuit. The electromagnetic interference conducted to secondary devices through CVT and CT in a substation has been studied in [12], and specific anti-interference measures have been put forward. Specialized researches about the CVT/CT reveal that the frequency responses of their transformation ratios exhibit serious nonlinear characteristics [13–15], and large error is inevitable when using the fundamental ratio to calculate the CEI level in the secondary circuit. However, none of the research on the secondary circuit CEI has considered a complete and accurate broadband equivalent circuit of CVT or CT.

The method for the analysis of the CEI characteristics on both the primary and secondary circuits in the UHVDC converter station is proposed in this paper, and its application in the Z-Q $\pm 800\,\mathrm{kV}/10000\,\mathrm{MW}$ UHVDC project is demonstrated in detail. The contributions of this paper include: 1) It provides comprehensive and thorough analysis of the CEI characteristic and its propagation in the primary circuit of a $\pm 800\,\mathrm{kV}/10000\,\mathrm{MW}$ UHVDC system under various scenarios; 2) This paper proposes to integrate complete and accurate BECs of the CVT and CT for the first time, to improve the accuracy of the CET characteristics analysis at the ports of the secondary circuit devices further.

The remainder of this paper is structured as follows. In Section 2, the basic information of the target UHVDC project is introduced, and the whole BEC of the UHVDC system is established. Section 3 and Section 4 present the analysis of the CEI characteristics in the primary circuit and the CEI characteristics under different operation modes of the UHVDC system, respectively. Section 5 establishes the BECs of the CVT, CT and secondary signal cable. The analyses of the voltage and current CEI characteristics at the ports of the secondary circuit devices are presented in Section 6 and Section 7, respectively. Section 8 addresses implications and potential concerns of this paper. Finally in Section 9, the main findings of this paper are summarized.

2. OVERALL BROADBAND EQUIVALENT CIRCUIT OF THE UHVDC SYSTEM

2.1. Basic in Formation of the Z-Q UHVDC Project

The Z-Q UHVDC project, starting from eastern Inner Mongolia, via Inner Mongolia, Hebei, Tianjin and Shandong province, ending in Shandong, is characterized by a $\pm 800\,\mathrm{kV}$ DC voltage level, 10000 MW bipolar transmission capacity, about 1200 km transmission length, 2 newly built converter stations with the sending end station in Zhalute and the receiving end station in Qingzhou, respectively.

Each converter station is constructed by two series 12-pulse converters ($400\,\mathrm{kV} + 400\,\mathrm{kV}$) per polar, and each series 12-pulse converter is located in a separate valve hall, thus each station has a total of four valve halls, i.e., the positive/negative high/low voltage halls, as shown in Fig. 1. The voltage between the high voltage lead-out wire of the converter to ground can be $400\,\mathrm{kV}$ or $800\,\mathrm{kV}$, which facilitates the UHVDC system to operate in different modes as needed, such as the bipolar full voltage, bipolar mixed voltage, bipolar/monopolar reduced voltage, and monopolar with metallic or ground return.

Each valve hall has 6 valve towers (3 towers per 6-pulse converter), and each valve tower is composed of 4 series valve modules (2 modules per valve leg). Each module contains 2 valve subassemblies, and a valve assembly is constructed by 15 series 6250 A SCRs, two saturated reactors and a shunt capacitor.

The rated no-load DC voltage of a 6-pulse converter of the Zhalute rectifier station and the Qingzhou inverter station are $230\,\mathrm{kV}$ and $216.6\,\mathrm{kV}$, respectively. Considering the 65 kA short-circuit current the
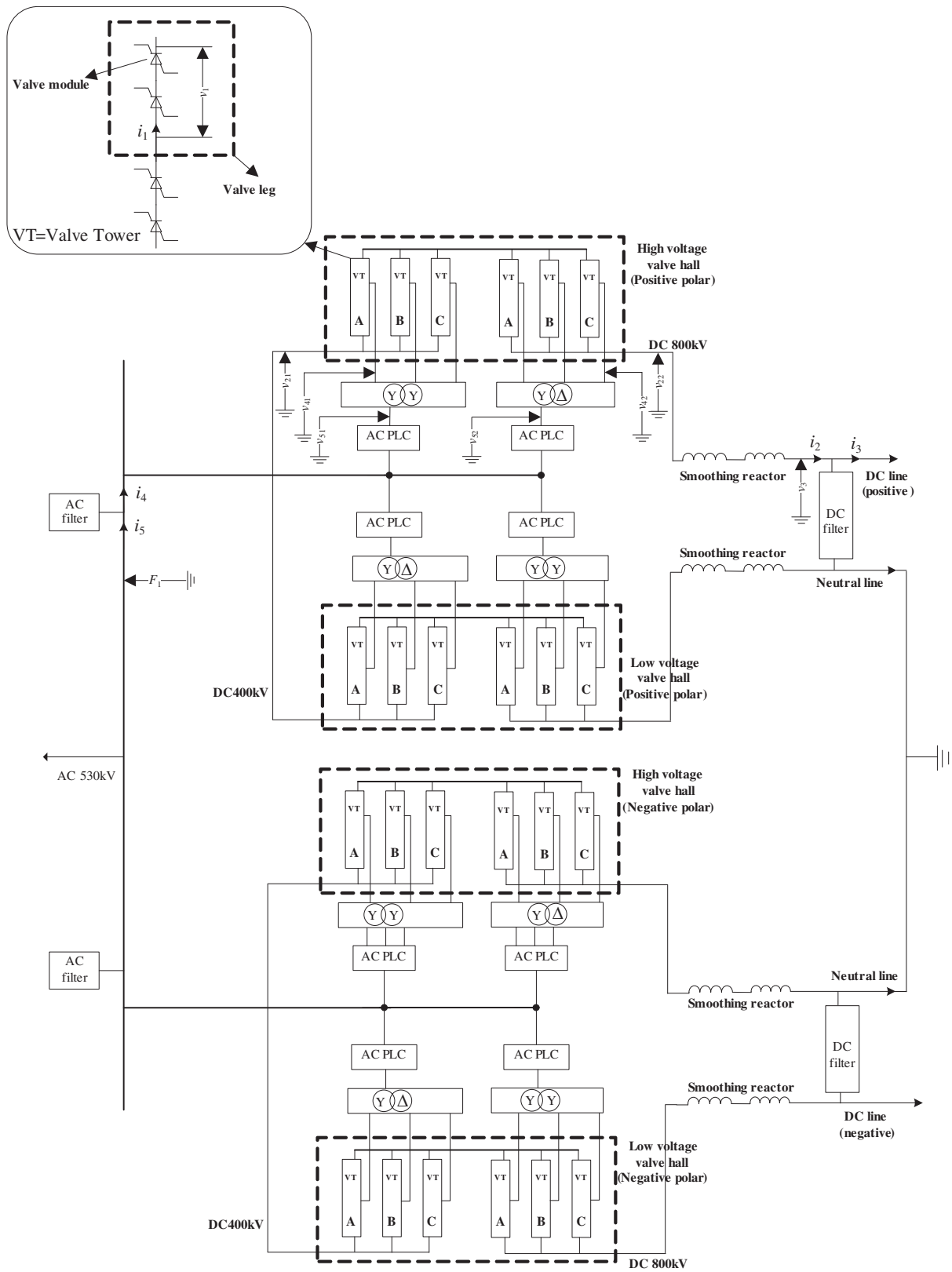
Figure 1. Structure of the Zhalute converter station.

converter valve to withstand, the calculated short-circuit impedances of the converter transformers of the Zhalute and Qingzhou stations are 16.65% and 16.58%, and the final design values are 18% and 17%, respectively. The converter-side line-to-line voltages of the transformers of the Zhalute and Qingzhou station are 170.3 kV and 160.4 kV, respectively. The calculated converter-side line-to-line current of the transformer of both the stations is 5.1 kA, thus the rated capacities of the single-phase two-winding converter transformers of the two stations are 501.8 MVA and 472.5 MVA, respectively.

Considering the 1200 km transmission line length and 10000 MW power transmission capacity of this project, the DC line adopts aluminium conductor steel reinforced with the specification $6 \times$ LGJ-900/40, and in the final scheme, the smoothing reactor with the same inductance value 2×75 mH is designed to install in each polar outlet and neutral outlet.

The numbers and types of the AC/DC filter banks to be equipped with in a converter station should consider the harmonic distribution characteristic during the operation of the UHVDC system and the investment and maintenance costs of these filters. Fig. 2 shows the types and structures of the designed AC/DC filter banks.
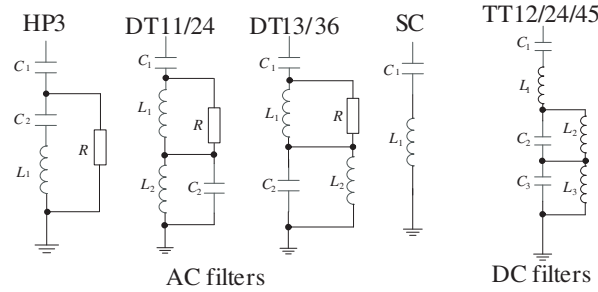
Figure 2. Structure of the filter banks.

2.2. BEC of the Converter Hall

Figure 3(a) shows the BEC of a 6250 A valve assembly, which is composed of SCRs, water-cooled resistor, saturated reactor, voltage sharing capacitor and RC snubber circuit. As introduced in above subsection, in a converter station each converter valve hall contains 6 valve modules, and the BEC of a hall is built by coupling the BECs of these valve modules via parasitic capacitances, as shown in Fig. 3(b).
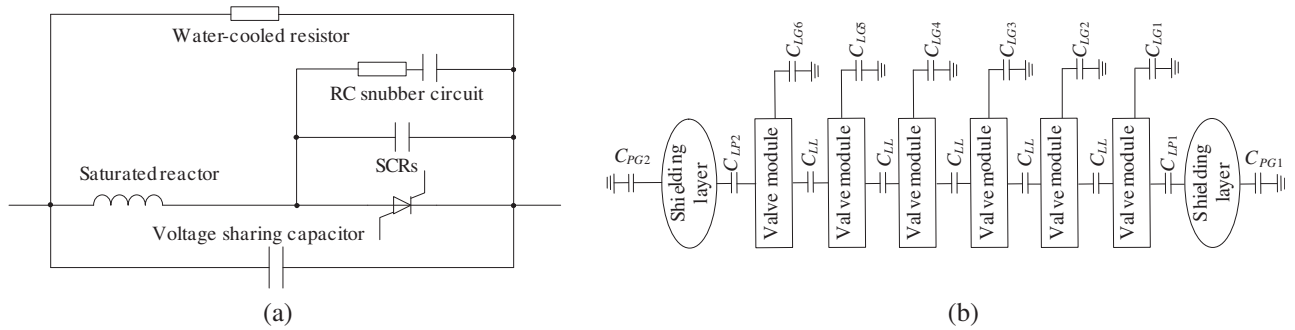
Figure 3. BEC of a converter hall of a converter station. (a) BEC of a valve assembly. (b) BEC of a valve hall.

2.3. BEC of the Converter Transformer

Figure 4 shows the BEC of a single-phase two-winding converter transformer. Excitation impedance (R_m, L_m) and leakage impedance $(R_{k1}, L_{k1}, R_{k2}, L_{k2})$ on primary and secondary sides represent the lower frequency response characteristic of the transformer, while the higher frequency response
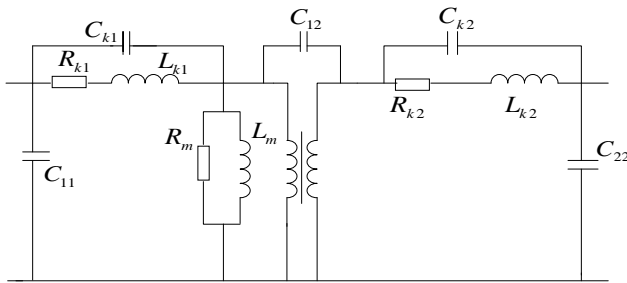
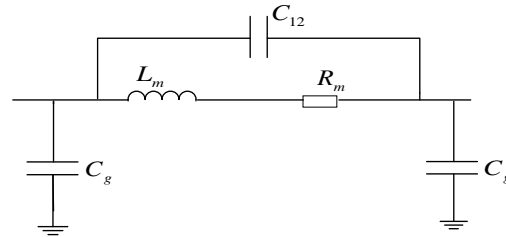**Figure 4.** BEC of the converter transformer.

Figure 5. BEC of the smoothing reactor.

characteristic is mainly dominated by several parasitic capacitances, including the primary and secondary winding-to-ground parasitic capacitances C_{11} and C_{22}, the parasitic capacitance C_{12} between these two windings, and the interturn capacitance (C_{k1}, C_{k2}) of each winding itself.

2.4. BEC of the Smoothing Reactor

The BEC of a smoothing reactor mainly consists of the main inductance L_m, power loss resistance R_m, terminal-to-ground parasitic capacitance C_g and interturn capacitance C_{12}, as shown in Fig. 5.

2.5. BEC of the AC PLC Filter Bank

The AC PLC filter should be installed at the system-side of the converter transformer, as shown in Fig. 1, and Fig. 6 is the BEC of this filter bank.
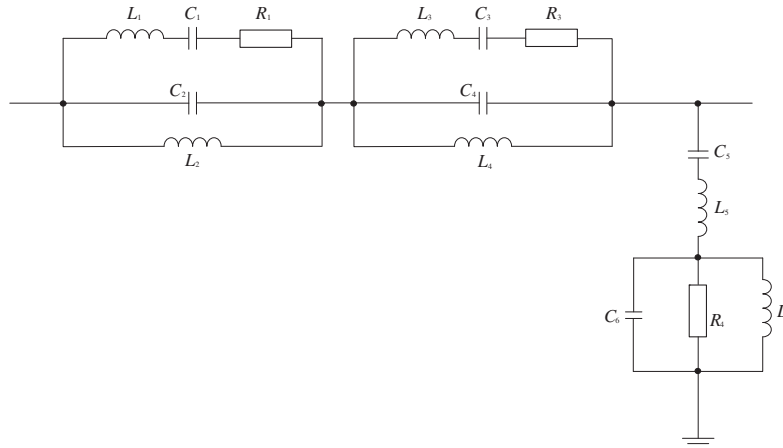

Figure 6. BEC of the PLC filter.

3. ANALYSIS OF THE CEI CHARACTERISTICS IN THE PRIMARY CIRCUIT

The broadband equivalent simulation model of the Z-Q UHVDC system has been built using PSCAD software based on the built BEC of the individual elements, and the frequency domain characteristics of the voltage and current are obtained by conducting FFT on the simulated time domain waveforms.

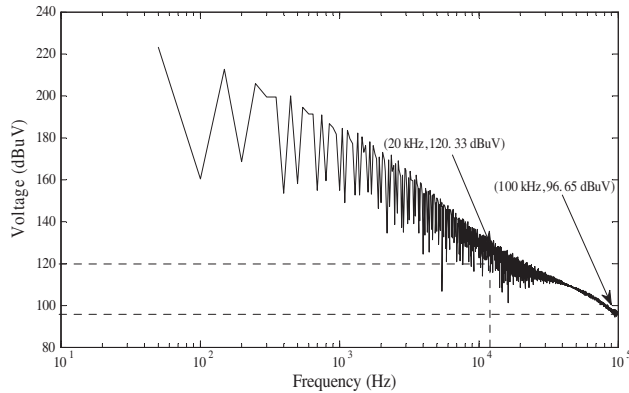### 3.1. CEI Characteristics of a Valve Leg

Figure 7 shows a typical frequency characteristic of the voltage (i.e., v_1 shown in Fig. 1) across a valve leg in a fundamental frequency period under the normal operation of the UHVDC system. Analysis of

the time-domain waveform shows that the voltage of the valve leg changes very drastically. The voltage change rate at the instance of the valve leg conducting exceeds $62.8 \text{ kV}/\mu s$, and it is about $19.8 \text{ kV}/\mu s$ at the instance of blocking. Simulation results of a $\pm 500 \text{ kV}$ HVDC system show that the values of these two indices are $40 \text{ kV}/\mu s$ and $15 \text{ kV}/\mu s$, respectively [16]; therefore, it can be roughly concluded that the electromagnetic interference level of a $\pm 800 \text{ kV}$ UHVDC converter station is about 30% higher than that of a $\pm 500 \text{ kV}$ HVDC system.

As seen from Fig. 7, the voltage CEI of the valve leg sourcing from the switching of SCRs presents a broadband feature. Its level decreases with the increase of the frequency in a wide frequency range and drops from $120.33 \text{ dB}\mu\text{V}$ to $96.65 \text{ dB}\mu\text{V}$ in the frequency range of 20 kHz–0.1 MHz. Research shows that in the same frequency range, the CEI levels of the valve leg of a $\pm 500 \text{ kV}$ HVDC system and the Yunnan-Guangdong (Y-G for short hereafter) $\pm 800 \text{ kV}$ UHVDC system drop from $125.3 \text{ dB}\mu\text{V}$ to $66.5 \text{ dB}\mu\text{V}$ and from $134.5 \text{ dB}\mu\text{V}$ to $91.7 \text{ dB}\mu\text{V}$ [17], respectively. Therefore, the voltage CEI level of the Z-Q converter station is certainly much higher than that of any existing UHVDC/HVDC system.

Figure 8 illustrates the frequency characteristics of the current (i.e., i_1 shown in Fig. 1) in a valve leg under the normal operation of the UHVDC system. It can be learned that the current in a valve leg has the same change rate of $3.125 \text{ kA}/\mu s$ at the instance of valve leg conducting and blocking, which is about 35% higher than the $2.3 \text{ kA}/\mu s$ of a $\pm 500 \text{ kV}$ HVDC system.

As seen from Fig. 8, the level of the current CEI of the valve leg drops from $90.12 \text{ dB}\mu\text{A}$ to $74.03 \text{ dB}\mu\text{A}$ in the frequency range 20 kHz–0.1 MHz. As a comparison, the CEI levels of a $\pm 500 \text{ kV}$ HVDC system and the Y-G project decrease from $83.9 \text{ dB}\mu\text{A}$ to $48.3 \text{ dB}\mu\text{A}$ and from $91.7 \text{ dB}\mu\text{A}$ to $51.1 \text{ dB}\mu\text{A}$ in the same frequency range, respectively, which again implies a more severe challenge coming from the electromagnetic interference field that the target UHVDC system is to withstand.

Figure 7. Voltage CEI characteristics of a valve leg.
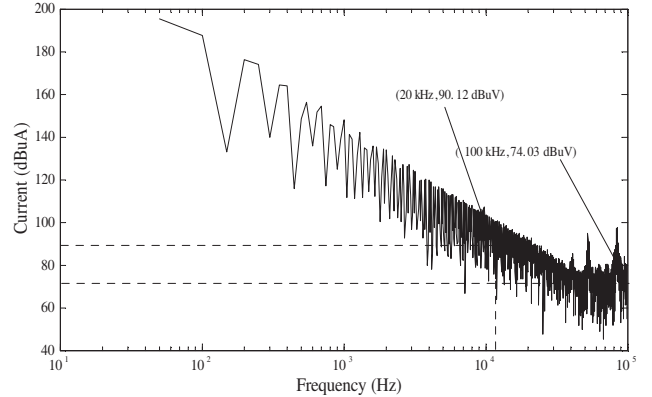
Figure 8. Current CEI characteristics of a valve leg.

3.2. CEI Characteristics of the DC Polar Outlet

Taking the positive polar as an example, Fig. 9 and Fig. 10 respectively show the frequency spectrums of the voltage and current of the DC outlet of the high voltage valve hall (800 kV) and low voltage valve hall (400 kV) under the normal operation of the UHVDC system.

It can be seen from Fig. 9 that for the DC outlet of the low voltage valve hall, the CEI level of the voltage (i.e., v_{21} shown in Fig. 1) drops from $124.09 \text{ dB}\mu\text{V}$ to $104.9 \text{ dB}\mu\text{V}$ in the frequency range 20 kHz–0.1 MHz, and that of the current decreases from $76.8 \text{ dB}\mu\text{A}$ to $71.49 \text{ dB}\mu\text{A}$. Simulation results of the Y-G UHVDC system reveal that the voltage and current CEI levels at the same place decrease from $109.8 \text{ dB}\mu\text{V}$ to $99.4 \text{ dB}\mu\text{V}$ and from $66.4 \text{ dB}\mu\text{A}$ to $49.3 \text{ dB}\mu\text{A}$, respectively.

As for the high voltage valve hall, Fig. 10 shows that the CEI level of the voltage (i.e., v_{22} shown in Fig. 1) drops from $129.89 \text{ dB}\mu\text{V}$ to $110.76 \text{ dB}\mu\text{V}$ in the frequency range 20 kHz–0.1 MHz, which is much higher than the $114.3 \text{ dB}\mu\text{V}$ to $86.0 \text{ dB}\mu\text{V}$ in the Y-G project. And the current CEI level decreases from $82.59 \text{ dB}\mu\text{A}$ to $69.4 \text{ dB}\mu\text{A}$, which is also much higher than $65.6 \text{ dB}\mu\text{A}$ to $54.7 \text{ dB}\mu\text{A}$ of the Y-G system.
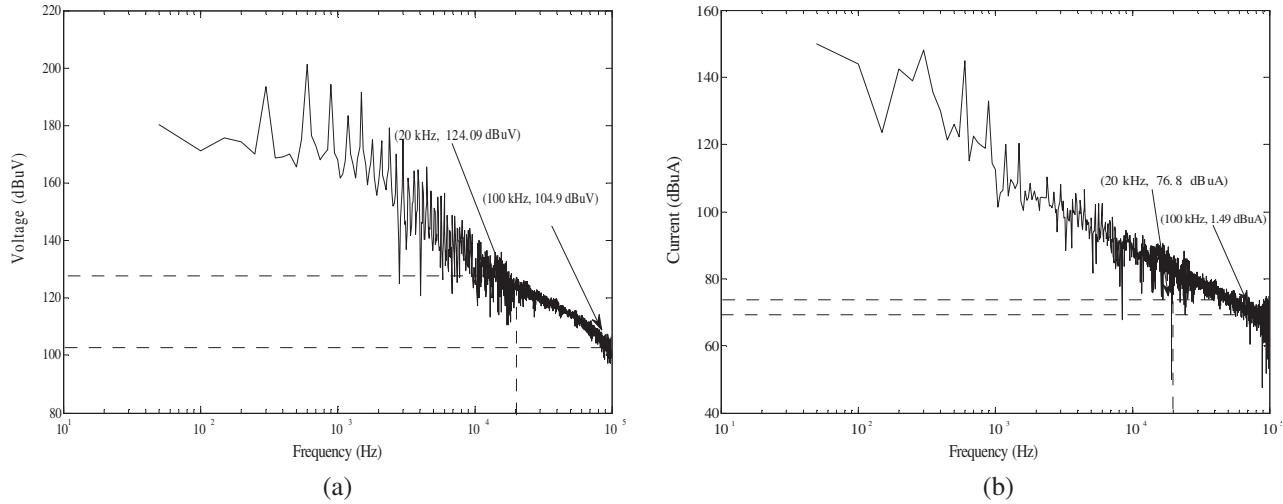
Figure 9. CEI characteristics of the DC outlet of the low voltage valve hall. (a) Voltage. (b) Current.
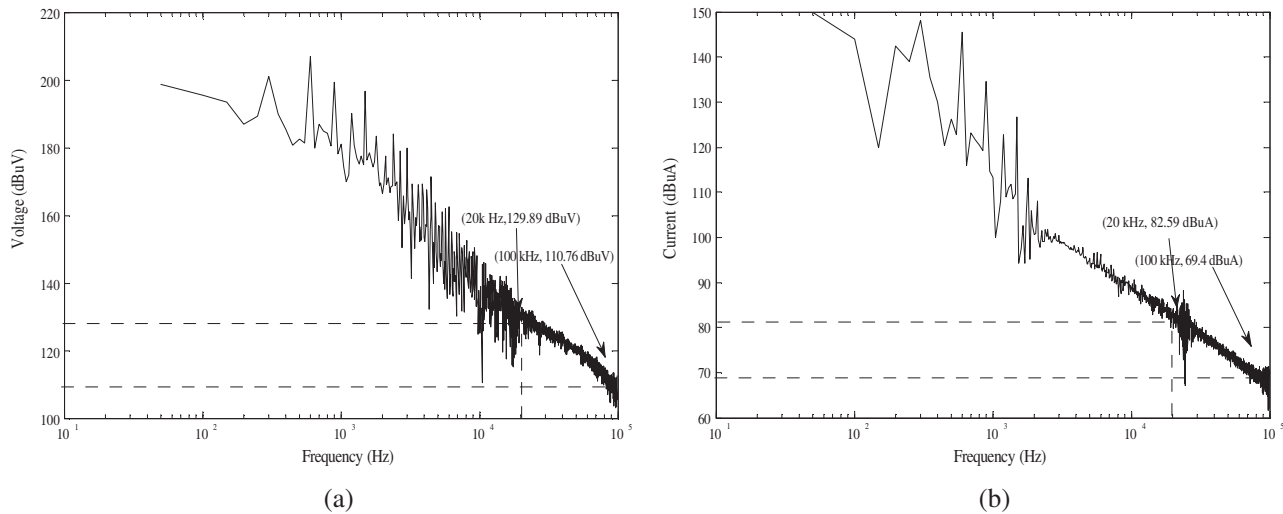

Figure 10. CEI characteristics of the DC outlet of the high voltage valve hall. (a) Voltage. (b) Curren.
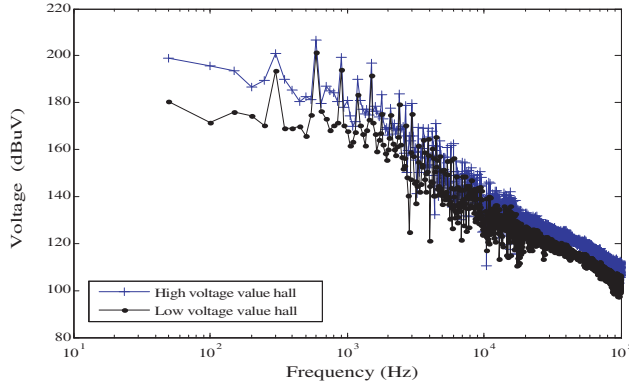
Figure 11 shows the comparison of the voltage CEI levels of the two valve halls outlets of the positive polar of the Zhalute converter station.

As seen from Fig. 11, the voltage CEI level of the high voltage valve hall outlet is higher than that of the low voltage one, due to the higher level and larger change rate of the voltage of the former.
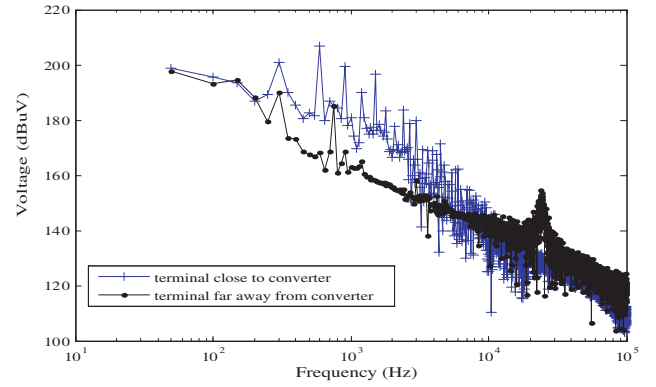
3.3. Influence of the Smoothing Reactor

From Fig. 1 we can see that four groups of smoothing reactors are equipped in Zhalute converter station to protect the converter valve from being damaged by the overvoltage stress and to depress the ripple in the DC current. Fig. 12 shows the CEI levels of the voltages (i.e., v_{22} and v_3 shown in Fig. 1) at the two terminals of the smoothing reactor in the positive polar DC line. Table 1 lists the specific values of the voltage CEI levels of the terminals of the smoothing reactor and the attenuations on the voltage CEI level at several typical frequencies.

From Table 1 we can learn that the smoothing reactor has a significant depress effect on the propagation of the voltage CEI due to its high impedance and the existing stray capacitance, and it

Figure 11. Comparison of the CEI levels of the two valve hall outlets.

Figure 12. Voltage CEI levels at the terminals of the smoothing reactor.

Table 1. Voltage CEI levels at the terminals of the smoothing reactor (dBμV).

Frequency (kHz)	20	40	50	60	70	80	90	100
v_{22}	129.8	122.3	120.1	119.2	117.8	112.1	110.4	110.8
v_3	123.5	111.9	104.8	104.6	98.9	102.8	95.9	94.2
Attenuation	6.3	10.4	15.3	14.6	18.9	9.3	14.5	16.6

can attenuates the voltage CEI level by 6.3 dBμV–18.9 dBμV when the voltage interference conducts from the DC polar outlet to the DC line. As a comparison, the voltage CEI attenuation level of the smoothing reactor in a ±500 kV HVDC system is 5.1 dBμV–18.2 dBμV, and that in the Y-G UHVDC project is 15.3 dBμV–20.4 dBμV.
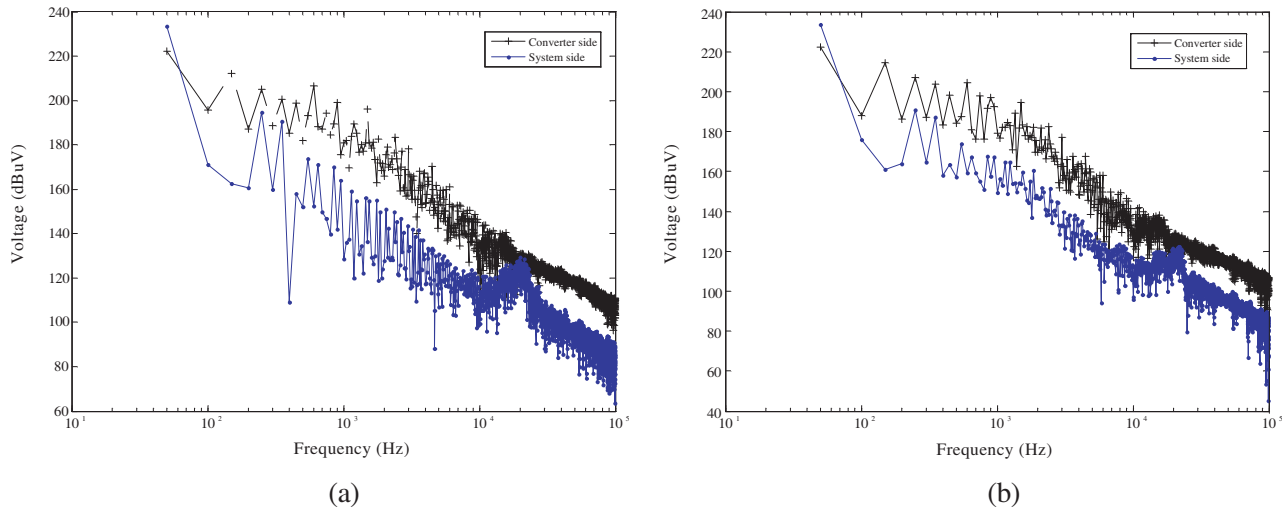
3.4. Influence of the Converter Transformer

Similar to the smoothing reactor, the converter transformer can also depress the voltage CEI level to a certain extent when the voltage CEI conducts from converter valve to the AC system of the station. Fig. 13 illustrates the voltage CEI characteristics at both the system- and converter-sides of the Y/Y and Y/Δ transformer of the Zhalute station. As shown in Fig. 1, v_{51} and v_{41} are the system- and converter-side voltages of the Y/Y transformer, and v_{52} and v_{42} are the system- and converter-side voltages of the Y/Δ transformer, respectively.

From Fig. 13 we can conclude that although both types of converter transformers can restrain the conduction of the voltage CEI, the attenuation levels are quite different. For the Y/Δ transformer, the attenuation level is 2.21 dBμV–32.43 dBμV, while that of the Y/Y transformer is 1.76 dBμV–38.93 dBμV. This difference comes from the difference in the parameter values of the stray elements in the BECs of these two transformers. As a comparison, the attenuation levels of the voltage CEI of the Y/Δ and Y/Y transformers in the Y-G project are 13.6 dBμV–28.8 dBμV and 8.2 dBμV–11.4 dBμV, respectively.

The current CEI characteristics of the system- and converter-sides of the Y/Y and Y/Δ transformers are shown in Fig. 14.

It can be seen from Fig. 14 that the attenuation levels of the current CEI of the Y/Δ and Y/Y transformers are 13.58 dBμA–17.49 dBμA and 9.46 dBμA–10.87 dBμA respectively, while those of the Y/Δ and Y/Y transformers in the Y-G project are 14.6 dBμA–31.4 dBμA and 6.5 dBμA–18.3 dBμA, respectively.

Figure 13. Voltage CEI levels at both sides of the converter transformer. (a) Y/Δ transformer. (b) Y/Y transformer.
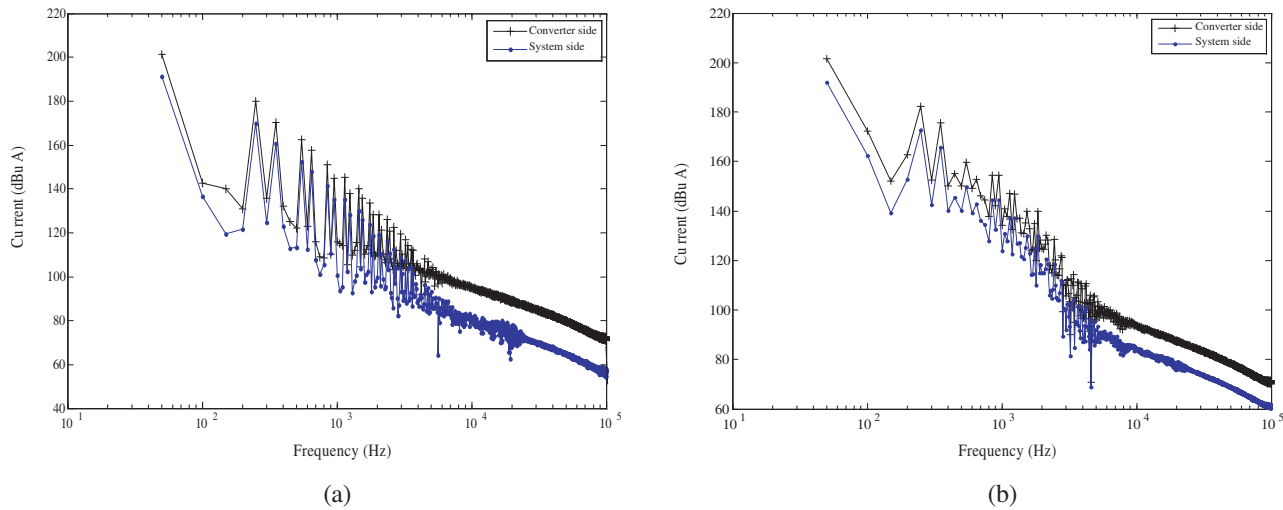
Figure 14. CurrentCEI levels at both sides of the converter transformer. (a) Y/Δ transformer. (b) Y/Y transformer.
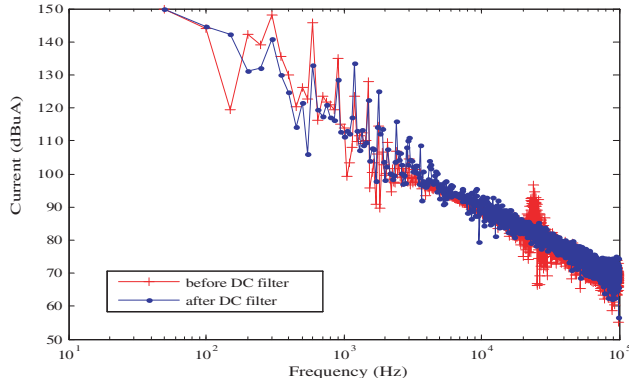
3.5. Influence of the AC/DC Filter Banks

Z-Q UHVDC system adopts two banks of TT12/24/45 three-tuned DC filter. The CEI characteristics of the currents before and after (i.e., i_2 and i_3 shown in Fig. 1) the DC filter bank under the normal operation of the UHVDC system are shown in Fig. 15.

Simulation result conforms that the DC filter can hinder the propagation of the CEI of the DC current, especially for the current component with the characteristic frequency of the 12-pulse converter, i.e., the attenuation levels of the 12th and 48th harmonic components are 13.68 dBμA and 11.4 dBμA, respectively, while that of the other individual component is below 5 dBμA.

Similarly, the AC filter banks, of which the types and structures are shown in Fig. 2, can attenuate the AC current CEI when it conducts to the AC bus. The CEI characteristics of the currents before and after (i.e., i_4 and i_5 shown in Fig. 1) the AC filter bank under the normal operation of the UHVDC system are shown in Fig. 16.
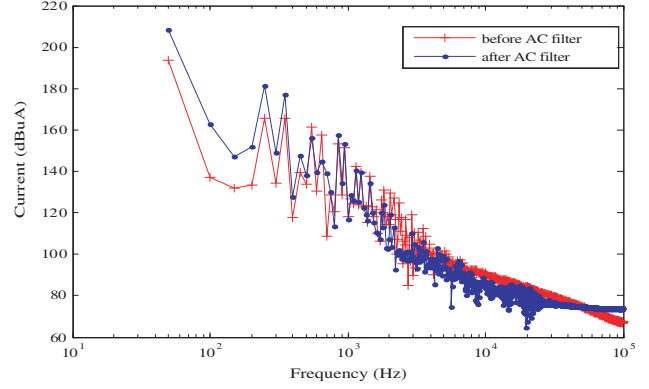
We can know from Fig. 16 that AC filter banks have a certain attenuation effect on the AC current CEI especially in the low frequency range, and the attenuation level is 2 dBμA–23.13 dBμA.

Figure 15. Current CEI levels before and after the DC filter bank.

Figure 16. Current CEI levels before and after the AC filter bank.

3.6. Influence of the PLC Filter Bank

Figures 17 and 18 show the voltage and current CEI levels at the system-sides of the Y/Y and Y/Δ converter transformers with and without the PLC filter, respectively. Table 2 lists the corresponding CEI levels and the influence of the PLC filter on the CEI at several typical frequencies in the frequency range of 10 kHz–0.5 MHz.

(a)

(b)
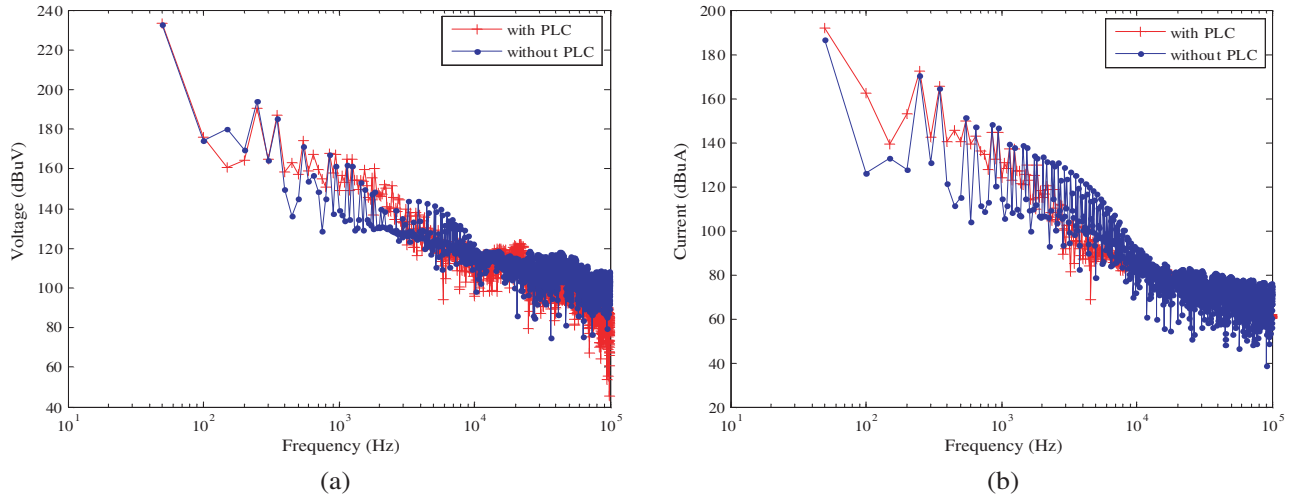
Figure 17. CEI characteristics of the system side of the Y/Y transformer. (a) Voltage CEI level. (b) Current CEI level.

As seen from above figures and Table 2, the AC PLC filter has a significant influence on the propagation of both the current and voltage CEIs, especially in the frequency range higher than 20 kHz. The PLC filter of the Y/Δ transformer can attenuate the voltage and current CEI levels on system-side of the transformer by 5.82 dBµV–25.62 dBµV and 5.45 dBµA–15.34 dBµA, respectively, while those of the Y/Y transformer are 4.43 dBµV–37.45 dBµV and 0.6 dBµA–9.85 dBµA, respectively. As for the Y-G UHVDC project, the corresponding attenuation levels are 5.1 dBµV–22.4 dBµV and 4.8 dBµA–28.7 dBµA for the Y/Δ transformer, and 5.1 dBµV–22.4 dBµV and 1.1 dBµA–23.4 dBµA for the Y/Y transformer, respectively.

(a)   (b)
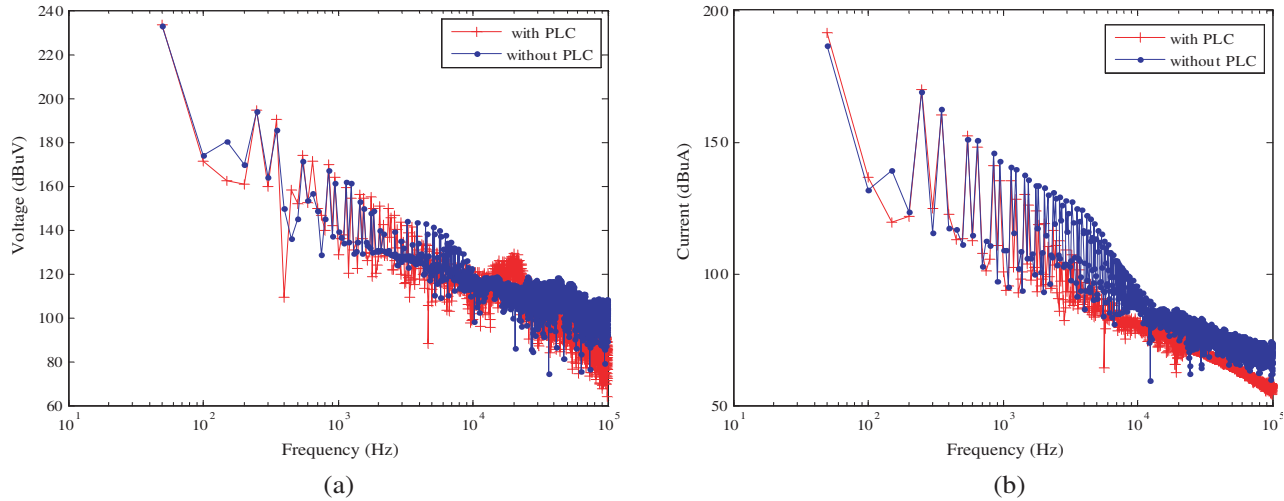
Figure 18. CEI characteristics of the system side of the Y/Δ transformer. (a) Voltage CEI level. (b) Current CEI level.

Table 2. Influence of the PLC filter on the CEI levels (dBμA or dBμV).

	Type	Frequency (kHz)	20	40	50	60	70	80	90	100
Current	Y/Δ	with	71.03	66.88	64.89	62.56	61.30	58.46	57.33	57.74
		without	81.04	72.33	74.43	74.90	73.11	73.80	71.48	72.95
		attenuation	10.01	5.45	9.54	12.34	11.81	15.34	14.15	15.21
	Y/Y	with	76.30	70.97	68.83	66.75	64.94	62.74	60.7	61.47
		without	80.38	72.81	76.66	71.49	74.79	63.95	61.311	70.71
		attenuation	4.08	1.84	7.83	4.74	9.85	1.21	0.6	9.24
Voltage	Y/Δ	with	126.14	99.52	99.31	89.80	83.66	88.17	85.53	79.10
		without	111.31	105.34	105.92	110.08	96.28	107.04	106.65	104.72
		attenuation	−14.83	5.82	6.61	20.28	12.62	18.87	21.12	25.62
	Y/Y	with	119.79	100.91	96.66	91.89	83.81	85.80	86.43	67.27
		without	111.31	105.34	105.92	110.08	96.28	107.04	106.65	104.72
		attenuation	−8.48	4.43	6.26	18.19	12.47	21.24	20.22	37.45

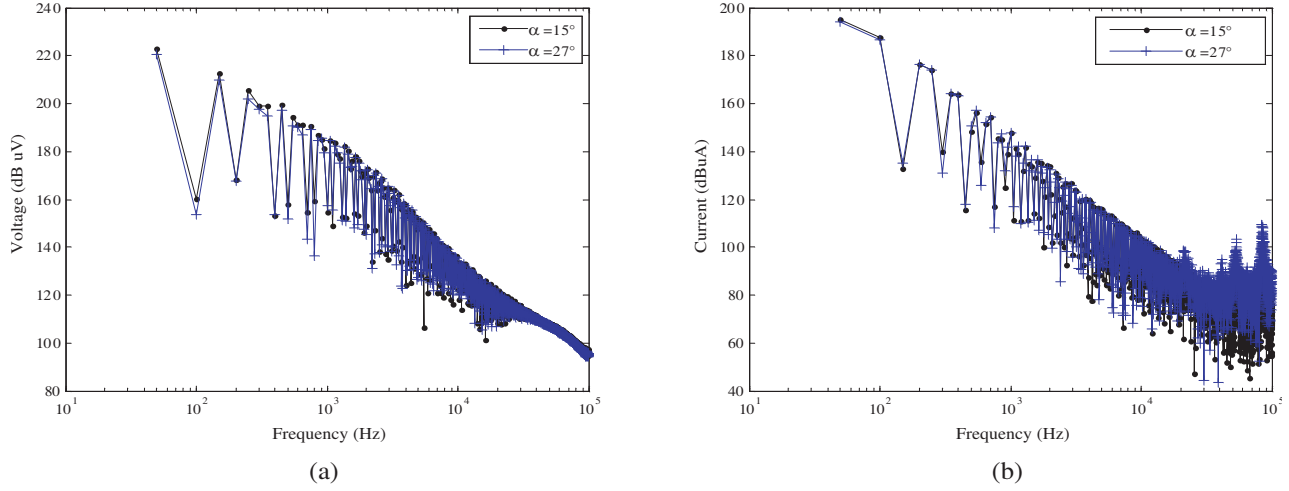## 4. CEI CHARACTERISTICS UNDER OTHER SITUATIONS

4.1. CEI of the Converter Valve with Different Firing Angles

Firing angle is an important factor determining the voltage and current waveforms of the converter valve, thus affecting the voltage and current CEI level in the UHVDC converter station. Fig. 19 shows the voltage and current CEI levels of a valve leg with the firing angles 15° (rated value) and 17°.

From Fig. 19 we can see that the larger the firing angle is, the higher the voltage and current CEI levels of a valve leg are, and this trend is more distinguish in the frequency range above 1 kHz. This phenomenon is mainly due to the increase in the load and power loss of the filter banks and converter transformer with a larger firing angel of the converter valve.

In this situation, the converter valve bears a higher voltage stress, thus causes a larger voltage and current CEI level on both the AC and DC sides of the converter valve. Therefore, the CEI characteristics under a larger firing angle should be considered when designing the anti-electromagnetic interference measures in the UHVDC converter station.

(a)

(b)

Figure 19. CEI characteristics of a valve leg with different firing angles. (a) Voltage CEI level. (b) Current CEI level.

4.2. CEI characteristics under Different Operation Modes

The Z-Q UHVDC converter station is characterized by a two-polar two series 12-pulse converter, which provides the system with flexible and diversified operation modes. Fig. 20 illustrates the voltage and current CEI levels of the valve leg under several typical operation modes of the system, including: the bipolar full/70% reduced voltage, monopolar full/70% reduced voltage with ground or metallic return, etc. Table 3 lists the voltage CEI levels of the converter leg and AC bus at several typical frequencies under these operation modes.

(a)

(b)
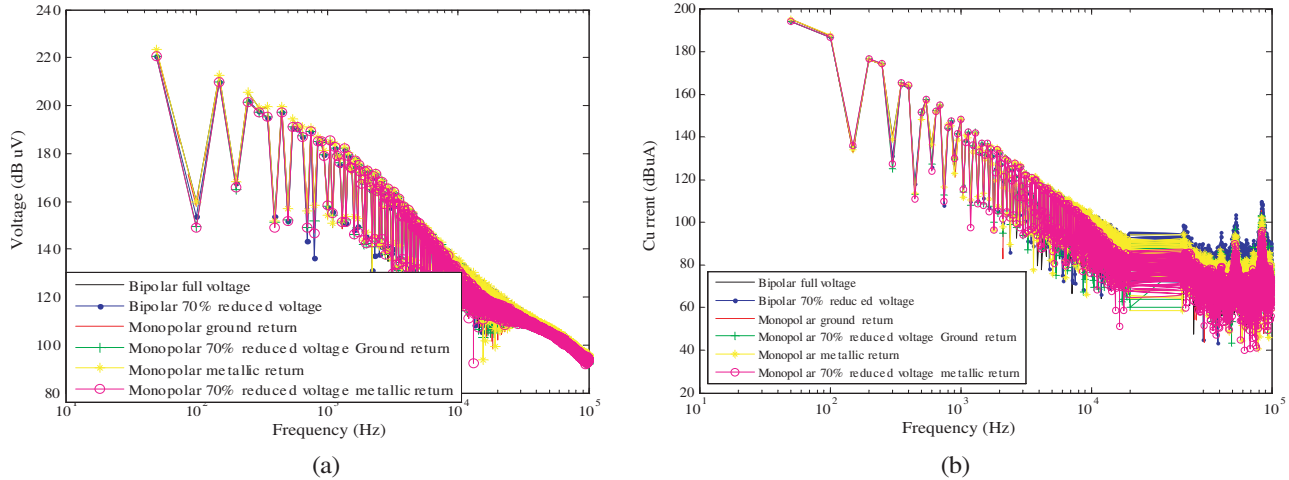
Figure 20. CEI characteristics of the valve arm under different operation modes. (a) Voltage CEI. (b) current CEI.

We can draw some meaningful conclusions from Fig. 21 and Table 3 that both the voltage CEI levels of the converter leg and AC bus: 1) under bipolar mode are higher than those under monopolar mode; 2) under full voltage mode are higher than those under reduced voltage mode; and 3) under monopolar ground return mode are lower than those under monopolar metallic return mode in the frequency range below 60 kHz, while the situation is just the opposite when the frequency is higher than 60 kHz.

Table 3. Voltage CEI levels of the converter valve/AC bus under different operation modes (dBµV).

| Frequency (kHz)	Bipolar full voltage	Bipolar 70% reduced voltage	Monopolar ground return	Monopolar 70% reduced voltage ground return	Monopolar metallic return	Monopolar 70% reduced voltage metallic return
20	120.33/126.14	120.10/128.82	117.15/104.89	114.92/97.51	116.46/103.64	114.86/92.71
40	110.26/99.51	109.56/91.67	106.95/97.46	108.33/89.02	109.65/94.70	107.24/88.17
50	107.84/99.31	107.49/87.70	105.28/94.73	105.44/85.91	107.59/91.96	104.92/85.45
60	105.74/89.80	104.66/80.53	102.36/91.96	102.78/83.29	104.21/89.61	102.44/82.58
70	103.06/83.66	101.82/78.14	100.32/88.86	100.51/80.81	101.99/86.71	100.05/79.78
80	100.48/88.17	99.33/75.55	98.58/85.16	96.95/76.80	97.97/83.72	97.00/75.76
90	97.14/85.53	96.38/85.37	97.64/79.01	94.48/71.57	96.69/81.13	94.71/69.05
100	96.65/79.10	95.01/85.03	96.76/63.81	92.98/67.21	95.14/79.43	93.75/52.95

5. BROADBAND EQUIVALENT CIRCUIT OF CVT, CT AND SECONDARY CIRCUIT CABLE

The secondary equipments in the UHVDC converter station mainly consist of the station control, valve control, thyristor trigger, its on-line monitoring system, monitoring system for the DC system, and the AC/DC relay protection system. As for the propagation routes of the electromagnetic interference, on the one hand, the CEI on the primary circuit may transmit to the secondary circuit via the coupling devices such as CVT and CT, causing interference to the secondary equipments. On the other hand, high intensity electromagnetic field will spread in the space of the valve hall and disturbs the normal operation of the secondary devices via the so called electromagnetic radiation form. This paper focuses on the analysis of the CEI characteristics at the ports of the secondary devices, and to this end, the BECs of the CVT and CT, which are adopted for the monitoring and measurement purpose, are to be established firstly.
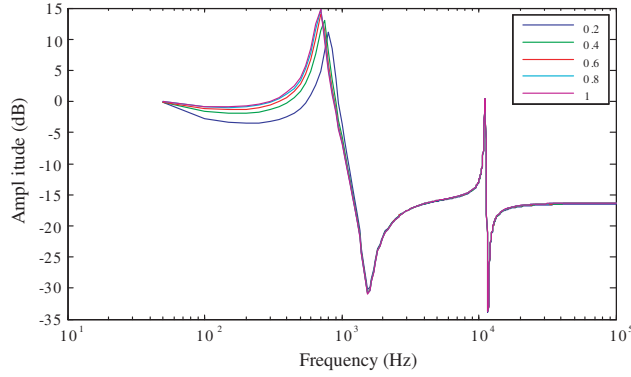
5.1. BEC of the CVT

A CVT is mainly composed of a capacitive voltage divider, electromagnetic unit and load. The capacitive voltage divider is made up of a high voltage and a medium voltage capacitor. The electromagnetic unit includes a compensation reactor, an intermediate transformer and a damper.

Under the system fundamental frequency, the CVT behaves as a voltage source with a constant amplitude under any load situation, due to the series resonance within the circuit formed by the compensation reactor and capacitive voltage divider. Converting the parameters of the secondary circuit elements into the primary side using the rated transformation ratio, the BEC of the CVT equipped in the AC bus of the Zhalute converter station is established in Fig. 21.
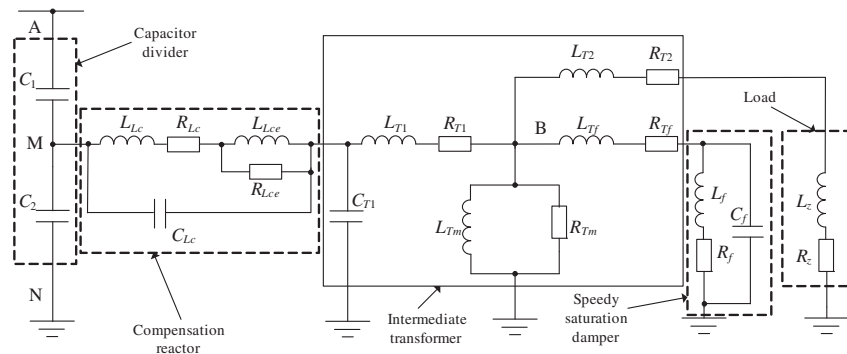
Figure 21. BEC of the CVT with speedy saturation damper.

Figure 22. Amplitude-frequency response of the transformation ratio of the CVT.
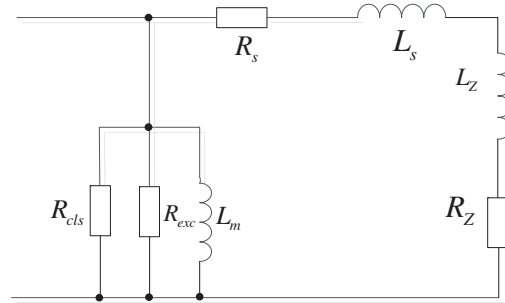
Figure 23. BEC of the CT.

In Fig. 21, C_1 and C_2 are high and medium voltage capacitors of the capacitor divider, respectively; L_{Lc} and R_{Lc} are the reactance and resistance of the compensation reactor; L_{Lce} and R_{Lce} are the reactance and resistance of the iron corn of this reactor; C_{Lc} is the stray capacitance; L_{T1} and R_{T1}, L_{T2} and R_{T2}, L_{Tf} and R_{Tf} are the reactance and resistance of the primary winding, measurement and protection winding, damper winding of the intermediate transformer, respectively. The measurement and protection winding have been merged as a whole due to their same capacity and output voltage level. L_{Tm} and R_{Tm} are the excitation reactance and resistance of the intermediate transformer. L_f, R_f, and C_f are the reactance, resistance and stray capacitance of the speedy saturation damper. The load of the CVT is represented by a reactance L_z in series with a resistance R_z. The stray capacitances of the secondary windings are ignored due to their relative small number of winding turns.

Figure 22 shows the amplitude-frequency response of the transformation ratio of the CVT, and the burden is at the rated capacity with a power factor 0.8 lagging.

The coordinates in Fig. 22 are in logarithmic scale, and the value of the vertical axis is the per unit value of the amplitude of the transformation ratio with the rated transformation ratio being the base value. Therefore, a value of 0 dB means that the transformation ratio is at its rated value.

From Fig. 22 we can see that the frequency response of the CVT exhibits a serious nonlinear characteristic, and the amplitude of the transformation ratio remains at its rated value (0 dB) only in a very narrow frequency range around the fundamental frequency 50 Hz. In the frequency range from 50 Hz to about 1000 Hz, the amplitude is higher than 0 dB, while it is smaller than 0 dB under the frequencies above 1000 Hz. Current methods for calculating the CVT secondary side voltage simply divide the primary side voltage by the rated transformation ratio, thus the calculated secondary voltages in the frequency range 50 Hz–1000 Hz are higher than their actual values while those of the frequencies above 1000 Hz are smaller, thus degrades the analysis accuracy of the CEI characteristics of the secondary circuit.

5.2. BEC of the CT

Figure 23 shows the BEC of the CT used for measuring the AC system current of the Zhalute converter station.

In Fig. 23, the magnetizing impedance of the CT is composed by three paralleling elements, and resistances R_{cls} and R_{elc} represent the eddy-current loss and other stray loss, respectively; L_m is the nonlinear magnetizing inductance; R_s and L_s are the leakage resistance and inductance of the secondary side winding. The burden is simulated by R_B and L_B.

Figure 24 shows the amplitude-frequency response of the transformation ratio of the CT.

From Fig. 24 we can see that the amplitude of the transformation ratio remains at its rated value (0 dB) from the fundamental frequency 50 Hz to about 500 Hz and decreases with the increase of the frequency in the range above 500 Hz. Therefore, the amplitude of the current component with the frequency above 500 Hz calculated by dividing the primary side current by the rated transformation ratio is lower than the actual values.
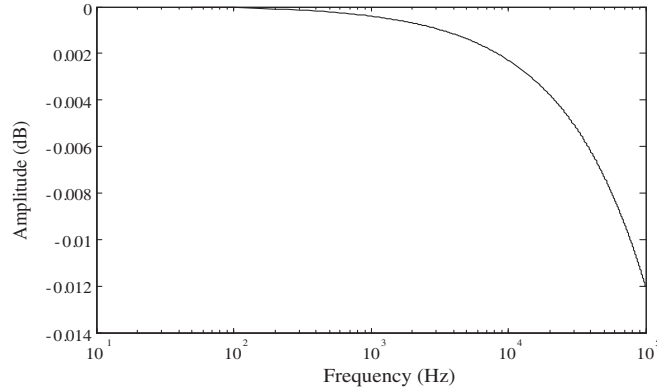
Figure 24. Amplitude-frequency response of the transformation ratio of the CT.
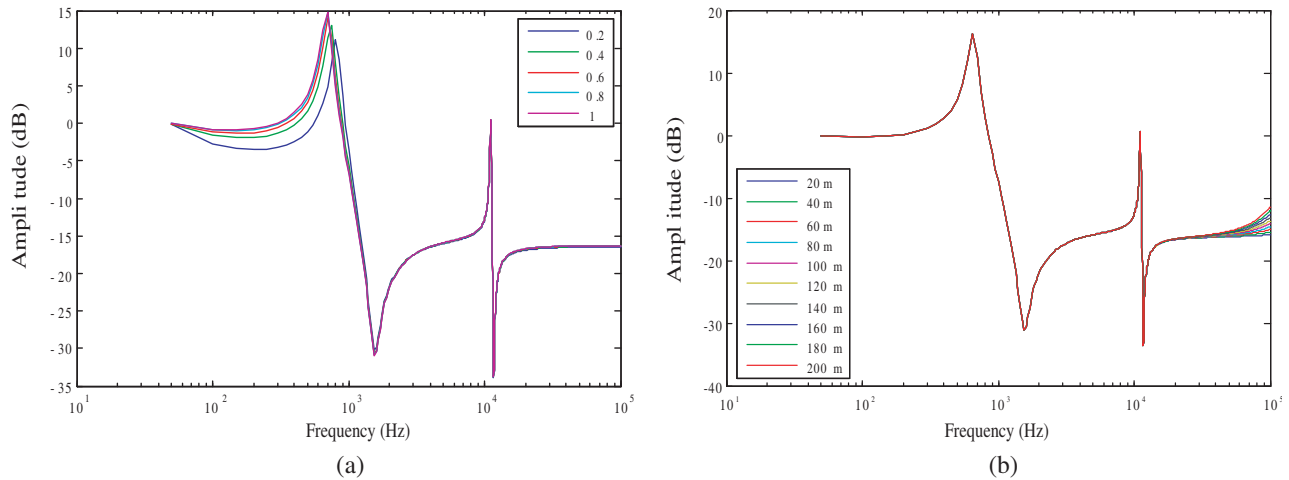

Figure 25. Influenceon the amplitude-frequency response of the transformation ratio of the CVT. (a) Influence of the burden rate. (b) Influence of the cable length.

5.3. BEC of the Secondary Circuit Signal Cable

According to the transmission line theory, the voltage and current of a secondary circuit signal cable simulated by a distributed parameter model can be expressed as:

$$\left(\begin{array}{c} \mathbf{U} \\ \mathbf{I} \end{array} \right) = \left(\begin{array}{cc} ch\left(\gamma x\right) & Z_c sh\left(\gamma x\right) \\ \frac{1}{Z_c} sh\left(\gamma x\right) & ch\left(\gamma x\right) \end{array} \right) \left(\begin{array}{c} \mathbf{U}_2 \\ \mathbf{I}_2 \end{array} \right) \tag{1}$$

where $\mathbf{U}_2$ and $\mathbf{I}_2$ are the voltage and current phasor at the end of the cable, respectively; $\mathbf{U}$ and $\mathbf{I}$ are the voltage and current phasors of the point with the distance x from the end of the cable; γ and Z_c are respectively the propagation constant and characteristic impedance of the cable.

By inserting the BEC of the signal table with the type KVVP22 into the BEC of the CVT shown in Fig. 22 and of the CT shown in Fig. 24 respectively, Fig. 25 and Fig. 26 reveal the influence of the cable length and burden rate on the amplitude-frequency characteristic of the CVT and CT, respectively.

From Fig. 25(a) we can learn that the burden rate mainly affects the amplitude of the transformation ratio of CVT in the frequency range of 50 Hz–1 kHz, thus mainly affects the low frequency voltage CEI characteristic in the secondary circuit, whereas the signal cable length mainly affects the amplitude of the transformation ratio in the frequency range above 50 kHz, as seen from Fig. 25(b).

In fact, there are ten curves in Fig. 26(a), and each curve corresponds to a burden rate with the value taken uniformly in the value range of 0–1.5. The overlapping of these curves implies that the burden rate has very slight influence on the amplitude of the transformation ratio of CT. From Fig. 26(b) we
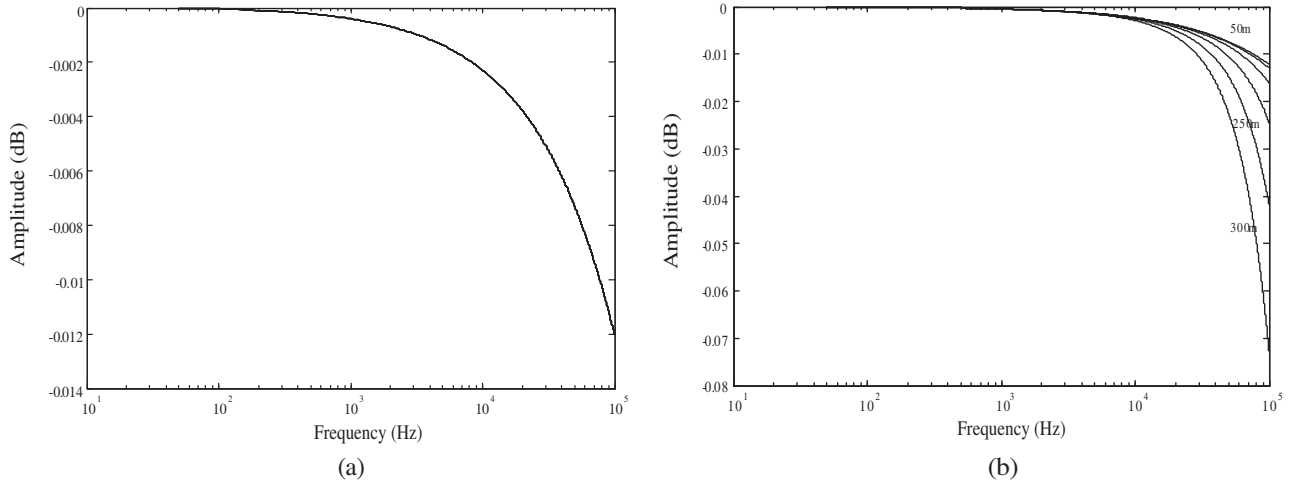
Figure 26. Influenceon the amplitude-frequency response of the transformation ratio of the CT. (a) Influence of the burden rate. (b) Influence of the cable length.

can learn that the cable length has an obvious impact on the amplitude of the transformation ratio in the frequency range higher than 50 kHz, thus affects the high frequency current CEI in the secondary circuit.

6. VOLTAGE CEI CHARACTERISTICS AT THE PORTS OF SECONDARY DEVICES

6.1. Under Steady State Operation

Figure 27 shows the voltage CEI levels at the ports of a secondary device under several steady state operation modes of the UHVDC system, and Fig. 28 illustrates the maximum voltage level at this port as a function of the cable length and burden rate.

As can be seen, with the decrease of the cable length and the increase of the burden rate, the voltage CEI level at the ports of this device will increase. According to the standard GB/T17626.6, the immunity of the secondary devices connected to the high voltage system should be class 3, i.e., the corresponding CEI level is 140 dBμV. From Fig. 31 we can know that the voltage CEI levels are less than 140 dBμV, which means that the CEI of the secondary device satisfies the requirement specified by the standard.
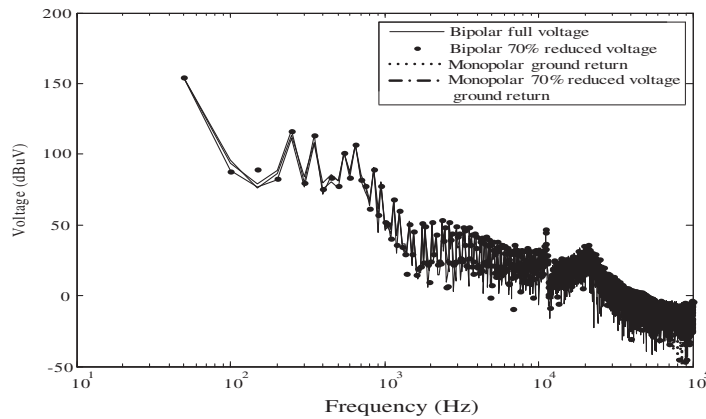
Figure 27. Voltage spectrum at secondary circuit under different operation modes.
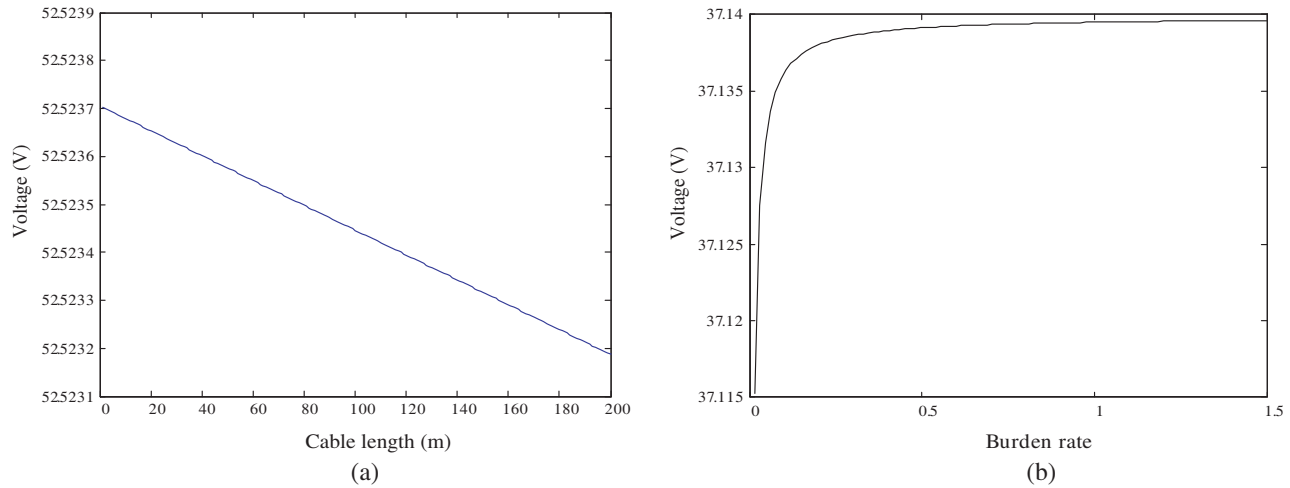
Figure 28. Maximum voltage level vs. the cable length and the burden rate. (a) Cable length. (b) Burden rate.
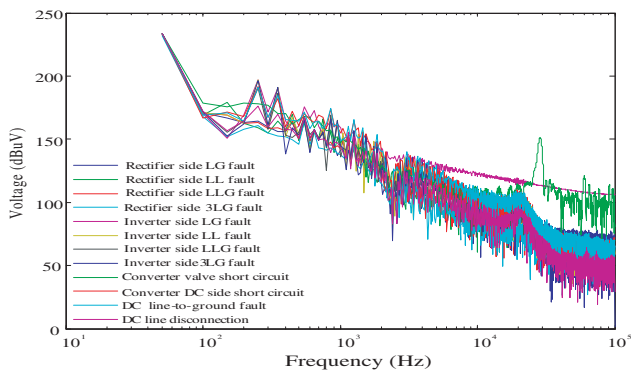
Figure 29. Voltage CEI levels at the device ports during system fault.
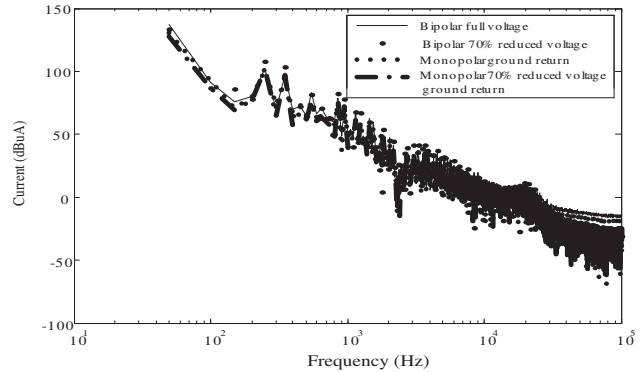
Figure 30. Current spectrum at secondary signal port under different operation modes.

6.2. During System Faults

The voltage CEI levels at the ports of a secondary device for different types of faults in the UHVDC system are shown in Fig. 29. We can learn from this figure that in the frequency range of 20 kHz–30 kHz, the voltage CEI level at the secondary device port during a converter valve short-circuited fault is the highest, whereas it is highest during a single-phase line-to-ground fault in the inverter station AC system bus over the other frequency range.

According to the provisions in the standard IEC6100-2-5, an interference with the degree of class 3 (corresponding to a voltage level of 3 V) is allowed at the port of a DC power supply, and that permitted for a signal/control device is class 4 (corresponding to a voltage level of 10 V) by compromise. We can known from Fig. 29 that in the frequency range of 0.1–30 MHz, the voltage interference level at the port of a signal/control device is certainly below 10 V, which meets the requirement in IEC6100-2-5.

## 7. CURRENT CEI CHARACTERISTICS AT THE PORTS OF SECONDARY DEVICES

7.1. Under Steady State Operation

Figure 30 shows the current CEI levels at the ports of a secondary device under several steady state operation modes of the UHVDC system, and Fig. 31 illustrates the maximum voltage level at this port
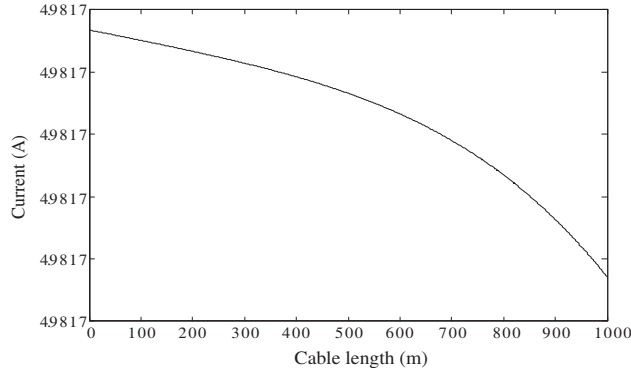
Figure 31. Maximum current level at the device ports vs. the cable length.

Figure 32. Current CEI levels at the device ports during system fault.

as a function of the cable length.

As can be seen, with the decrease of the cable length, the voltage CEI level at the ports of this device will increase.
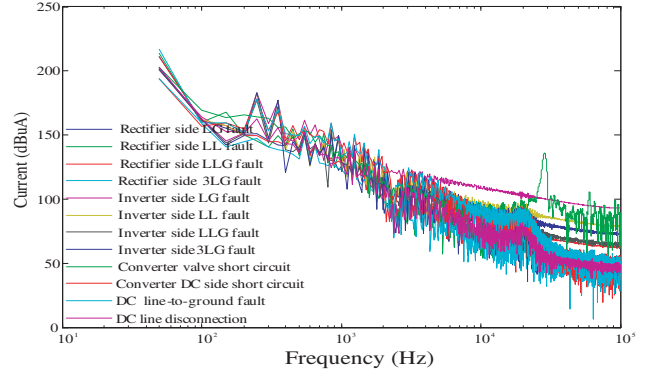
7.2. During System Faults

Figure 32 shows the current CEI levels at the ports of a secondary device during different types of faults in the UHVDC system.

Figure 32 shows that in the frequency range of 20 kHz–0.1 MHz, the current CEI level at the secondary device port during a inverter valve short-circuited fault is the highest, i.e., 103.66 dBμA–92.94 dBμA, whereas during a converter valve short-circuited fault and a DC side line-to-ground fault, the current CEI levels are 94.46 dBμA–64.21 dBμA and 91.74 dBμA–49.81 dBμA, respectively.

8. DISCUSSION

This paper is initiated to systematically examine and evaluate the CEI characteristics in the primary circuit and at the ports of the secondary devices of the converter station of the Z-Q UHVDC transmission system, which has the maximum power capacity among the UHVDC projects with the same voltage levels in China. By building the whole BEC of the converter station of this UHVDC project, the CEI levels of the primary circuit of the converter station under steady-state, system faults and different operation modes are analyzed quantitatively, and the CEI characteristics at the ports of the secondary devices under steady-state and system faults are analyzed accurately by the introduction of the BEC of the CVT and CT.

The voltage and current CEIs in the converter station originate from the conducting and turning-off process of the power electronic device of the converter valve. Simulation results show that the steady-state voltage and current CEI levels of the Z-Q project are certainly much higher than those of any existing UHVDC system and are about 30% higher than those of a ±500 kV HVDC system. It is worth noting that the CEI levels under system fault or larger firing angel operation are likely to exceed those under the normal operation. For example, the voltage CEI levels of the converter valve under a three phase short circuit fault on the rectifier station and a line-to-ground short circuit fault on the DC line increase by 20% and 33% in average compared with the levels under the normal operation of the system. The limits of the interference in existing EMI standards are specified for the steady-state operation, even though the system fault may be of a very short duration, but these higher levels of CEI should be considered emphatically in the updating of the relevant standards in the future.

Simulation results also verify that the primary circuit equipments of the converter station, such as the converter transformer, AC filter and PLC filter at the AC-side, the smoothing reactor and DC filter at the DC-side, have an important impact on the propagation of the CEI characteristics. These equipments can attenuate the voltage and/or current CEI levels by a certain extent, wherein the AC

PLC filter has the most distinct effect. Therefore, it is recommended that a UHVDC project with large power capacity shall be equipped with the PLC filter in its converter station in terms of EMI suppression.

The CEI on the primary circuit may transmit to the secondary circuit via the coupling devices such as CVT and CT, causing disturbing interference to the secondary equipments. None of the current research has recognized the influence of the frequency response of the transformation ratio of the CVT and CT on the propagation of the CEI, and just calculated the CEI levels on the secondary device circuit utilizing the rated transformation ratio. We reveal that the frequency responses of the CVT and CT exhibit a serious nonlinear characteristic. For example, the amplitude of the transformation ratio of the CVT remains at its rated value only in a very narrow frequency range around the fundamental frequency. In the frequency range from 50 Hz to about 1000 Hz, the amplitude is higher than the rated value, while it is smaller than the rated value under the frequencies above 1000 Hz. Table 4 compares the voltage CEI levels on the secondary circuit under different operation modes of the UHVDC system with and without the consideration of the nonlinear characteristic of the CVT.

Table 4. Comparison of the voltage CEI levels on the secondary device circuit (dBμV).

Frequency (kHz)	Bipolar full voltage			Bipolar 70% reduced voltage			Monopolar ground return		
	rated	actual	Error (%)	rated	actual	Error (%)	rated	actual	Error (%)
20	51.74	35.03	48	54.42	37.71	44	30.49	13.78	121
40	25.11	8.77	186	17.27	0.93	1758	23.06	6.72	243
50	24.91	8.60	190	13.30	−3.01	−542	20.33	4.02	405
60	15.40	−0.89	−1829	6.13	−10.16	−160	17.56	1.27	1283
70	9.26	−7.02	−232	3.74	−12.54	−130	14.46	−1.82	−894
80	13.77	−2.51	−649	1.15	−15.13	−108	10.76	−5.52	−295
90	11.13	−5.14	−316	10.97	−5.30	−307	4.61	−11.66	−139
100	4.70	−11.57	−141	10.63	−5.64	−288	−10.59	−26.86	−61
Frequency (kHz)	Monopolar 70% reduced voltage ground return			Monopolar metallic return			Monopolar 70% reduced voltage metallic return		
	rated	actual	Error (%)	rated	actual	Error (%)	rated	actual	Error (%)
20	23.11	6.40	261	29.24	12.53	133	18.31	1.60	1046
40	14.62	−1.72	−950	20.30	3.96	413	13.77	−2.57	−636
50	11.51	−4.80	−340	17.56	1.25	1302	11.05	−5.26	−310
60	8.89	−7.40	−220	15.21	−1.08	−1508	8.18	−8.11	−201
70	6.41	−9.87	−165	12.31	−3.97	−410	5.38	−10.90	−149
80	2.40	−13.88	−117	9.32	−6.96	−234	1.36	−14.92	−109
90	−2.83	−19.10	−85	6.73	−9.54	−170	−5.35	−21.62	−75
100	−7.19	−23.46	−69	5.03	−11.24	−145	−21.45	−37.72	−43

The data in the columns with the label 'rated' and 'actual' are, respectively, the voltage levels on the secondary circuit calculated by the rated and actual transformation ratio of the CVT. As we can learn from this table that by considering the nonlinear characteristic of the transformation ratio of the CVT, the accuracy of the analysis of the CEI levels on the secondary circuit has been improved effectively, thus it is beneficial to formulate EMI suppression measures with better focalization and scientificity.

Our work provides a universal way to understand the CEI characteristics in the primary circuit and at the ports of the secondary devices of the converter station of an UHVDC transmission system. Further field measurement of the CEI characteristics is warranted to improve the BEC model built in this study.

9. CONCLUSIONS

Based on the established BEC of a $\pm 800\,\text{kV}/10000\,\text{MW}$ UHVDC project, this paper researches the CEI characteristics of the primary circuit of a converter station systematically, and more importantly, the analysis accuracy of the CEI characteristics at the ports of secondary devices under different operation modes and different types of faults of the UHVDC system is improved greatly by the introduction of the BEC of CVT/CT. The model built and conclusions drawn in this paper have been used as the reference for designing the anti-interference measures of the secondary devices in the Zhalute converter station. The field measurement of the CEI characteristics and necessary improvements of the model will be conducted after the normal operation of the target system, and relevant research results will be presented in following papers.

REFERENCES

1. Kong, F., Z. Hao, and B. Zhang, "A novel traveling-wave-based main protection scheme for $\pm 800\,\text{kV}$ UHVDC bipoloar transmission lines," *IEEE Trans., PD.*, Vol. 31, 2159–2168, 2016.
2. Zhang, S., Z. Peng, P. Liu, and N. Li, "Design and dielectric characteristics of the $\pm 1100\,\text{kV}$ UHVDC wall bushing in china," *IEEE Trans., DEI.*, Vol. 22, 409–419, 2015.
3. Yang, Y., J. Lu, and Y. Lei, "A calculation method for the hybrid electric field under UHVAC and UHVDC transmission lines in the same corridor," *IEEE Trans., PD.*, Vol. 25, 1146–1153, 2010.
4. Li, Y., L. Luo, C. Rehtanz, C. Wang, and S. Ruberg, "Simulation of the electromagnetic response characteristic of an inductively filtered HVDC converter transformer using field-circuit coupling," *IEEE Trans., IE.*, Vol. 59, 4020–4031, 2012.
5. Zilberti, L., E. Pons, O. Bottauscio, M. Chiampi, and M. Pastorelli, "Evaluation of the electromagnetic environment around underground HVDC lines," *IEEE Trans., PD.*, Vol. 25, 3085–3094, 2010.
6. Yu, Z., Y. Fu, R. Zeng, F. Tian, M. Li, L. Liu, R. Li, and Z. Gao, "Data analysis of electromagnetic environment of UHVDC transmission lines," *IET International Conference on AC and DC Power Transmission*, 1–4, 2016.
7. Ma, Y., S. Li, Y. Hua, L. Yu, and P. Chen, "Reliability evaluation to converter transformers of 2×12-pulse UHVDC transmission system," *China International Conference on Electricity Distribution*, 219–222, 2014.
8. IEC 61000-4-6, "Electromagnetic compatibility-Part 4-6: Testing and measurement techniques-Immunity to conducted disturbances, induced by radio-frequency fields," 2013.
9. Sun, H., X. Cui, L. Liu, and L. Qi, "Simulation of conductive electromagnetic interference in HVDC converter station," *World Automation Congress*, 1–5, 2008.
10. Sun, H., X. Cui, and L. Du, "Electromagnetic interference prediction of $\pm 800\,\text{kV}$ UHVDC converter station," *IEEE Trans. Magn.*, Vol. 52, 1–4, 2015.
11. Yu, Z., J. He, and R. Zeng, "Simulation analysis on conducted EMD caused by valves in $\pm 800\,\text{kV}$ UHVDC converter station," *IEEE Trans. EC.*, Vol. 51, 236–244, 2009.
12. Dou, H. and Z. Liang, "Simulation of electromagnetic interference coupling to a substation secondary cable," *Asia-Pacific International Symposium on Electromagnetic Compatibility*, 1417–1420, 2010.
13. Ghassemi, F., P. F. Gale, B. Clegg, T. Cumming, and C. Coutts, "Method to measure CVT transfer function," *IEEE Trans., PD.*, Vol. 17, 915–920, 2002.
14. Ghassemi, F., P. Gale, T. Cumming, and C. Coutts, "Harmonic voltage measurements using CVTs," *IEEE Trans., PD.*, Vol. 20, 443–449, 2005.
15. Cataliotti, A., D. D. Cara, A. E. Emanuel, and S. Nuccio, "Current transformers effects on the measurement of harmonic active power in LV and MV networks," *IEEE Trans., PD.*, Vol. 26, 360–368, 2011.

16. Liu, L., X. Cui, Q. Wang, and H. F. Sun, "Measurement and calculation of the transient electromagnetic disturbances of secondary system in HVDC converter station," *2008 World, Automation Congress*, 1–4, 2008.

17. Sun, H. F., X. Cui, and L. Qi, "High-frequency modeling of valve components in high voltage direct current converter stations," *Transactions of China Electrotechnical Society*, Vol. 24, 142–148, 2009.